JOURNAL OF MATERIALS SCIENCE 21 (1986) 871–878

The influence of pearlite fraction on fracture toughness and fatigue crack growth in nodular cast iron

JI-LIANG DOONG, JIUN-REN HWANG, HSING-SHIH CHEN
Department of Mechanical Engineering, National Cheng Kung University, Tainan, Taiwan

Fracture toughness and fatigue crack growth data of four nodular cast irons with different pearlite fractions are studied. The influence of temperature on fracture toughness is also investigated. Fracture surfaces are observed using a scanning electron microscope to correlate fracture toughness with the fracture surface and to understand the mechanism of crack growth at different stress intensity factor ranges. It is shown that the upper shelf fracture toughness increases with pearlite fraction. The existence of nodular void regions on the fracture surface plays an important role in fracture toughness. The fatigue crack growth rate is less sensible to stress intensity factor range when pearlite fraction increases.

1. Introduction

It is important to obtain meaningful design data such as fracture toughness and fatigue crack growth rate of materials in predicting the fail-safe behaviour of metals. Due to the increasing use of nodular cast iron, it is necessary to study their fracture behaviour and obtain the relevant fracture data.

Nodular cast iron studies in the past few years can be divided into two fields.

1. The effects of graphite variables such as volume fraction, dispersion type and shape etc. Extreme results have been concluded on this. Xu [1] indicates that fracture toughness in pearlitic nodular cast iron increases with the refinement of the graphite nodules. On the other hand according to Holdsworth and Jolley [2] and Bradly and Mead [3, 4], the crack opening displacement at ductile crack initiation and fracture toughness are independent of graphite nodule count and volume fraction.

2. The effects of the properties of a steel-like matrix. Previous studies [2, 5–11] mainly focused on the different characteristics of ferritic grade and pearlitic grade cast iron. It is found that the pearlitic grade has a slightly higher fracture toughness than the ferritic grade. In [3, 4, 12], it is shown that the toughness parameter $(K_{Ic}/\sigma_y)^2$ increases with increasing ferrite fraction, where K_{Ic} is the fracture toughness and σ_y is the yield strength. Most of the above studies aim mainly at obtaining design data. They seldom correlate fracture toughness with the fracture surface. In addition, the effects of pearlite on fracture properties are still not clearly understood.

Crack initiation and propagation have become important topics recently. For nodular cast iron, the effects of matrix microstructure on the fracture mechanism have been studied by polishing techniques [13–17] and electron microscopy [15, 18], in which tensile specimens are used. Other samples, such as impact specimens [19–21] and bending specimens [22–24] have also been used. However, studies of fracture mechanism by using fatigue crack growth specimens are rare. The fatigue crack growth rate of nodular cast iron can be described by the Paris equation as $da/dN = C\Delta K^m$ [12]. For the ferritic and pearlitic grade, the values of m are 4.5 and 5.0, respectively [25]. For the pearlitic grade, different results (m = 3.5 to 4.2) are concluded in [1].

The aim of this paper is to study (a) the effects of pearlitic fraction on fracture toughness and fatigue crack growth rate, (b) the correlation between fracture toughness and fracture surface and (c) the fracture mechanism at different stress intensity factor ranges.

2. Experimental procedure

Four nodular cast irons were investigated in the present study. They were melted in a 20 kg high-frequency induction furnance, magnesia-treated in a ladle and cast into CO_2 moulds whose dimensions are 205 mm × 160 mm × 45 mm, feeder not included. Three of them, denoted as iron A, B and C in Table I are made with different ferrite and pearlite fractions among one another during the casting processes. Their pearlite fractions in the matrix are 4, 27 and 67%, respectively. The fourth iron with 97% pearlite in the matrix, denoted as iron D, is produced by a normalizing heat treatment (maintained at 930° C for 2 h, then air cooled to room temperature). Microconstituent percentages are measured with an image analysis system. The unetched specimen is used for measuring the graphite fraction. Then the specimen is etched and the total fraction of graphite and pearlite is measured. Finally, the percentage of pearlite or ferrite fraction in the matrix can be calculated. Chemical compositions and microconstituent percentages of all four irons are shown in Table I and their microstructures in Fig. 1. Since the variation in graphite variables of these irons are small, the effects of graphite are negligible.

0022–2461/86 $03.00 + .12

TABLE I Chemical compositions and microconstituent percentages

Iron	Chemical compositions (wt %)						Pearlite (%*)	Ferrite (%*)	Nodular count (mm^{-2})	Rate of spheroidization (%)
	C	Si	Mn	P	S	Mg				
A	3.64	2.32	–	0.028	0.012	0.055	4	96	117	96
B	3.60	2.31	–	0.027	0.010	0.047	27	73	104	97
C	3.67	2.40	–	0.029	0.007	0.051	67	33	112	96
D	3.63	2.38	–	0.030	0.009	0.049	97	3	115	95

*Graphite fraction is discounted.

The mechanical properties tests were performed in an MTS closed-loop hydraulic servo-controlled testing system. An environmental chamber filled with a mixture of alcohol and dry ice is used to keep the temperature within $\pm 1°C$, and centre-cracked specimens were used to measure the fracture toughness K_c and fatigue crack growth rate da/dN. The specimens configurations are shown in Fig. 2. The K_c measuring method suggested by John and William [26] is employed in the test. Specimens were precracked by fatigue, and loaded to fracture. The K_c value is calculated by the following equation [27]

$$K_c = [pc^{1/2}/(2tb)][1.77 - 0.1(c/b) + (c/b)^2] \quad (1)$$

where p is the fracture load, t is specimen thickness, b is half specimen width and c is half the crack length. The fracture surfaces were observed using a scanning electron microscope (SEM). Testing procedure of fatigue crack growth was in accordance with the standards of ASTM E647. A sinusoidal load was applied at a frequency of 15 Hz. The ratio of the minimum to the maximum load was equal to 0.05 throughout this study. Specimen surfaces are polished in order to produce optional conditions for identification of crack paths. The growing fatigue crack length is displayed on a $\times 25$ microscope with an accuracy of 0.05 mm. The machine can automatically indicate fatigue cycles, and the cyclic stress intensity at every moment of stressing can be calculated.

3. Results and discussion

The results of the tensile tests are shown in Fig. 3. In general, both the yielding strength and the tensile strength increase with decreasing temperature and with increasing pearlite fraction.

The plots of fracture toughness against temperature are shown in Fig. 4. For ferritic irons A and B, the K_c value increases as temperature decreases till a point at which the fracture mode changes to complete cleavage is reached. Iron C shows the transition behaviour in K_c value clearly. The upper limit of transition temperature range is used as a parameter for comparison, which coincides with the temperature at which the fracture surface completes its changing to 100% cleavage from the mixed mode of nodular void and cleavage. It is found that the transition temperatures of irons A, B, C and D are in the ranges of $T_A < -75°C$, $-75°C < T_B < -50°C$, $-50°C < T_C < -25°C$ and $25°C < T_D$, respectively. The upper shelf K_c values of the irons increase with increasing pearlite fraction, and the effect is more noticeable at higher pearlite content. This is similar to the tensile results.

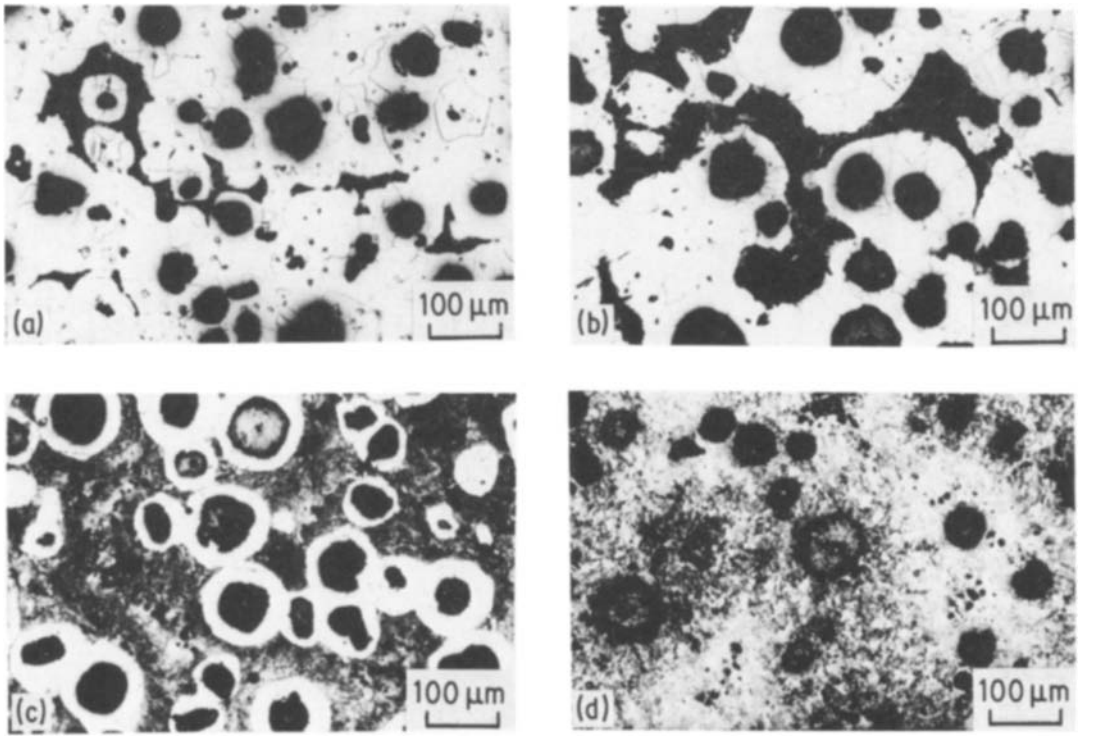

Figure 1 Microstructure of irons (a) A, (b) B, (c) C and (d) D.

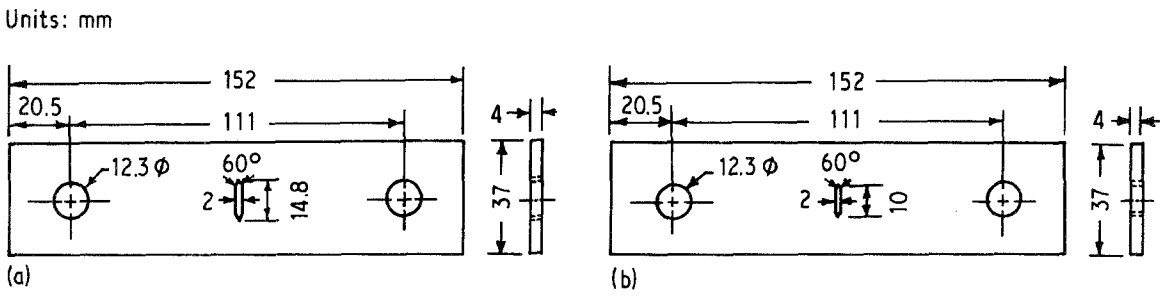

Figure 2 Specimen configurations for (a) fracture toughness and (b) fatigue crack growth.

Fracture toughness is affected by the combination of strength and toughness. As temperature decreases, a higher yield strength is obtained, and the resultant increase in fracture toughness may not indicate a tougher material. Therefore, the other toughness parameter K_c/σ_y may be used for evaluating the material toughness [6, 10]. The plots of K_c/σ_y against temperature are shown in Fig. 5. There are two characteristics which are opposite to that obtained from fracture toughness data (Fig. 4). Firstly, the K_c/σ_y values of ferritic iron A and iron B decrease with decreasing temperature. It means that the materials become more brittle as temperature decreases. Secondly, because of ferrite being tougher than pearlite, the K_c/σ_y value decreases with increasing pearlite fraction apparently.

The overload regions on the fracture surface of the fracture toughness specimens are divided into three subregions: the nodular void, the transgranular cleavage and the mixed mode of nodular void and transgranular cleavage. Fig. 6 shows the nodular void morphology of iron A. There is a higher nodule count with narrow internodule bridges fractured by chisel-point shear rupture. Dimple structures appear especially at large ferrite regions. With this type of fracture, high plastic deformation occurs, and higher energy is required for fracture. The transgranular cleavage of iron A is shown in Fig. 7. A river pattern is clearly observed. Owing to the crystalline orientations of the ferrite grains always being different, the cleavage direction changes at the grain boundaries. Because spheroidal graphite can retard the propagation of cleavage cracks, the crack path avoids passing through the graphite. Therefore, the amount of graphite observed in the cleavage region is much smaller than that in the nodular void region. The appearance of both the nodular void and the transgranular cleavage of iron B are similar to those of iron A. Fracture modes of iron C as shown in Figs. 8 and 9, have been discussed in a previous work [28]. Fig. 8 presents the mixed mode of nodular void and transgranular cleavage, and Fig. 9 presents two types of the cleavage. Large cleavage facets observed in iron D are shown in Fig. 10. The small light pots on the graphite surfaces

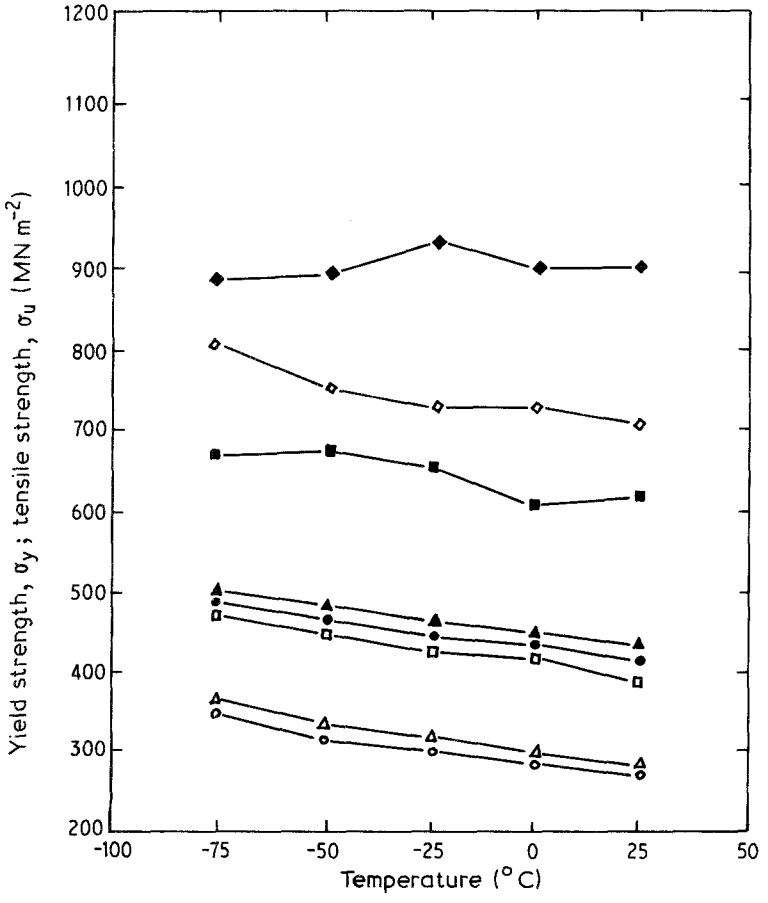

Figure 3 Plots of yield strength, σ_y, 0.2% offset (○ Iron A, △ Iron B, □ Iron C, ◇ Iron D) and tensile strength, σ_u (● Iron A, ▲ Iron B, ■ Iron C, ◆ Iron D) against temperature.

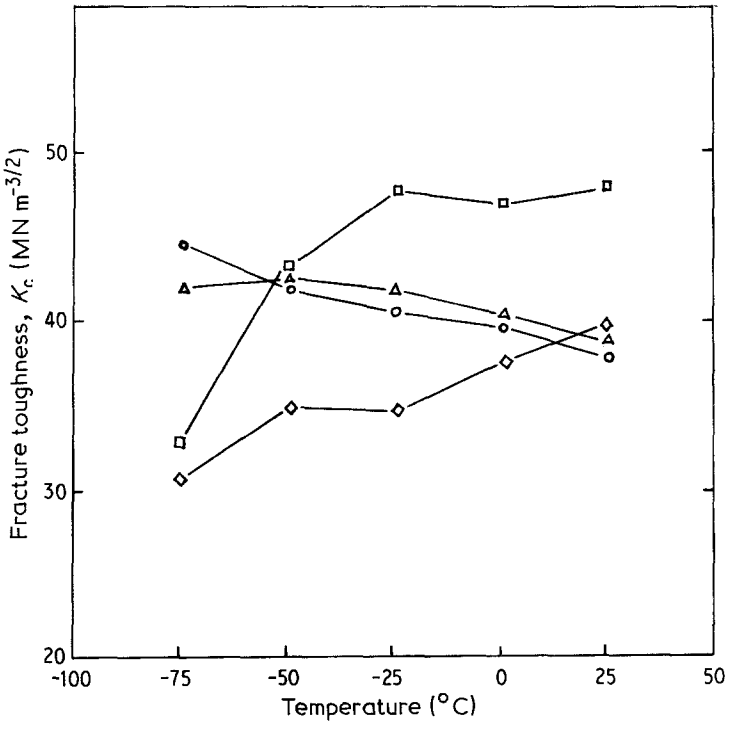

Figure 4 Plots of fracture toughness K_c against temperature. ○ Iron A, △ Iron B, □ Iron C and ◊ Iron D.

are temper carbons, the same results have been reported by Kuroda and Takada [24]. In addition, it should be noted that fracture never occurs within spheroidal graphite for the four irons. It always proceeds along the weak interface between graphite and the matrix.

The percentage of each fracture subregion on the fracture surface is given in Table II. The nodular void region indicates a ductile fracture mechanism and the transgranular cleavage region will be a brittle fracture mechanism. Shrinkage of the nodular void region is observed as the temperature drops down, but the transgranular cleavage region is the opposite to this. This characteristic explains the tendency of toughness data which decreases with temperature.

Fracture toughness is a measure of the resistance to unstable crack extension. The K_c/σ_y ratio represents the size of the plastic zone prior to unstable crack

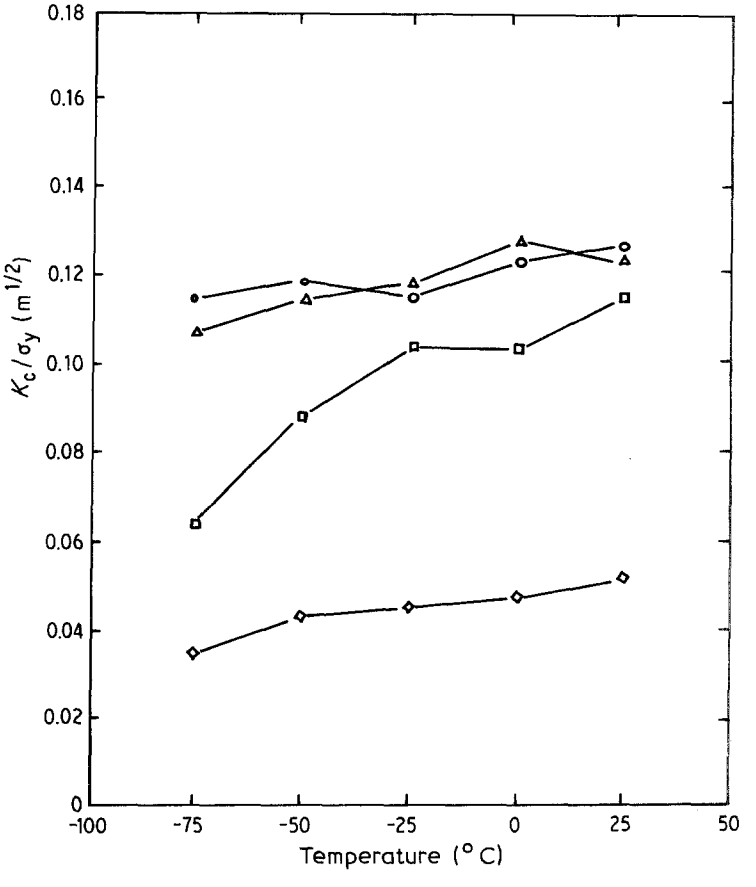

Figure 5 Plots of K_c/σ_y against temperature. ○ Iron A, △ Iron B, □ Iron C and ◊ Iron D.

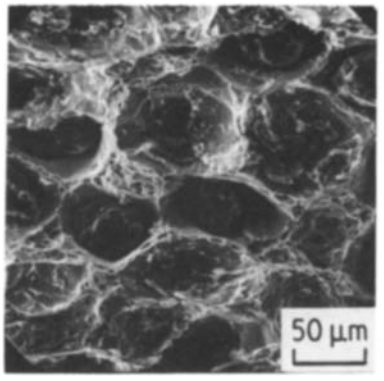

Figure 6 Nodular void of iron A.

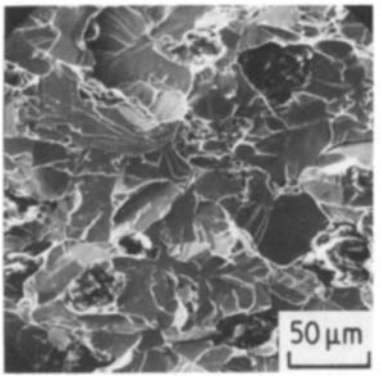

Figure 7 Transgranular cleavage of iron A.

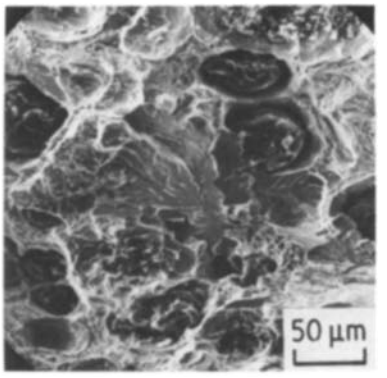

Figure 8 Mixed mode of nodular void and transgranular cleavage of iron C.

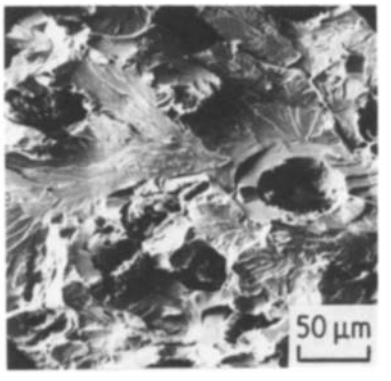

Figure 9 Transgranular cleavage of iron C.

growth. From the percentage of each fracture region on the fracture surface, the required energy for fracture can be predicted. Therefore, there must be some relationship existing among these parameters. For irons A and B, the percentage of nodular void region on the fracture surface decreases with decreasing temperature. This phenomenon indicates that a lower energy is required for fracture. It is also indicated by the K_c/σ_y curves, but not by the fracture toughness ones. This may be due to the increasing yield strength at lower temperature. This is why K_c/σ_y is usually used in comparing the toughness of materials. There is also an important phenomenon noted between the K_c value and the fracture surface of irons B and C. The fracture surface comes to 100% transgranular cleavage just as the K_c value of iron B begins to drop, or as the K_c value of iron C drops rapidly. In addition, it is found that the existence of a nodular void region

TABLE II The percentage of each fracture region on the fracture surface of fracture toughness specimen

Iron	Temperature (°C)	Nodular void (%)	Mixed mode of nodular void and transgranular cleavage (%)	Transgranular cleavage (%)
A	25	100	–	–
	0	100	–	–
	−25	100	–	–
	−50	15	–	85
	−75	–	6	94
B	25	100	–	–
	0	100	–	–
	−25	–	31	69
	−50	–	26	74
	−75	–	–	100
C	25	–	30	70
	0	–	19	81
	−25	–	9	91
	−50	–	–	100
	−75	–	–	100
D	25	–	–	100
	0	–	–	100
	−25	–	–	100
	−50	–	–	100
	−75	–	–	100

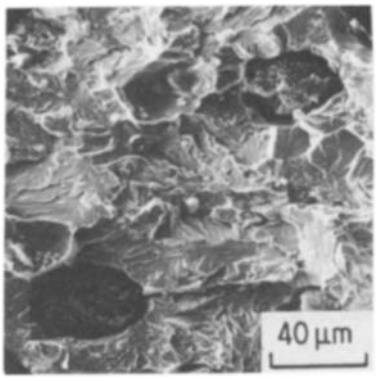

Figure 10 Transgranular cleavage of iron D.

plays a more important role than the size of the region does.

In Fig. 11, the fatigue crack growth rates are plotted as a function of stress intensity factor range on log–log axes for the irons at 25° C. The middle parts of the curves can be described the Paris equation as $da/dN = C(\Delta K)^m$ where C and m are material constants. The C and m values are given in Table III. From these results, we can see the material constants and crack growth data of iron D are similar to those given previously [1]. The exponent constant m apparently decreases when the pearlite fraction increases. This phenomenon indicates that crack growth rate is less sensitive to stress intensity factor range when the pearlite content increases. In general, the greater the pearlite fraction is, the lower the crack growth rate is. But for iron D, the crack growth curve is above the other curves. It may be due to the disappearance of the ferrite ring around the graphite which deforms to a large extent and reduces the stress concentration.

TABLE III Expression of da/dN, where ΔK has units of $MN\,m^{-3/2}$

Iron	C	m	da/dN (m/cycle)
A	1.19×10^{-14}	5.35	$1.19 \times 10^{-14}\,\Delta K^{5.35}$
B	1.80×10^{-14}	5.08	$1.80 \times 10^{-14}\,\Delta K^{5.08}$
C	2.95×10^{-14}	4.73	$2.95 \times 10^{-14}\,\Delta K^{4.73}$
D	3.08×10^{-13}	4.28	$3.08 \times 10^{-13}\,\Delta K^{4.28}$

The fracture surfaces of the fatigue crack growth specimens are observed, and it is possible to correlate the surface morphology to the fatigue crack data plots. The characteristics of the fatigue crack surfaces of both irons A and B are similar. Intergranular fracture is observed at a lower level of ΔK as shown in Fig. 12. When ΔK increases, the transgranular fracture portion increases, and the mixed mode of intergranular and transgranular fracture appears, as shown in Fig. 13. At still higher ΔK values, fatigue striations are visible as shown in Fig. 14. The irregular directions of the fatigue striations indicate the random local microcrack growth. This is due to the existence of graphite which acts as a hole [29, 30] and increases the local stress intensity factor. The direction of microcrack growth is towards the graphite. In addition, after the crack grows along the interface between the graphite and the matrix, a new microcrack is initiated and propagated. The new microcrack growth direction is not always the same as the origin. Fig. 15 shows the fracture surface of iron C at a lower ΔK value. Two distinct areas with clear interfaces are observed. The intergranular fracture in the ferrite ring, and the shear fracture in the pearlite colonies. As ΔK increases, the interface becomes less distinct. Fig. 16 shows this case. The fracture surface of iron D at a lower ΔK value is shown in Fig. 17.

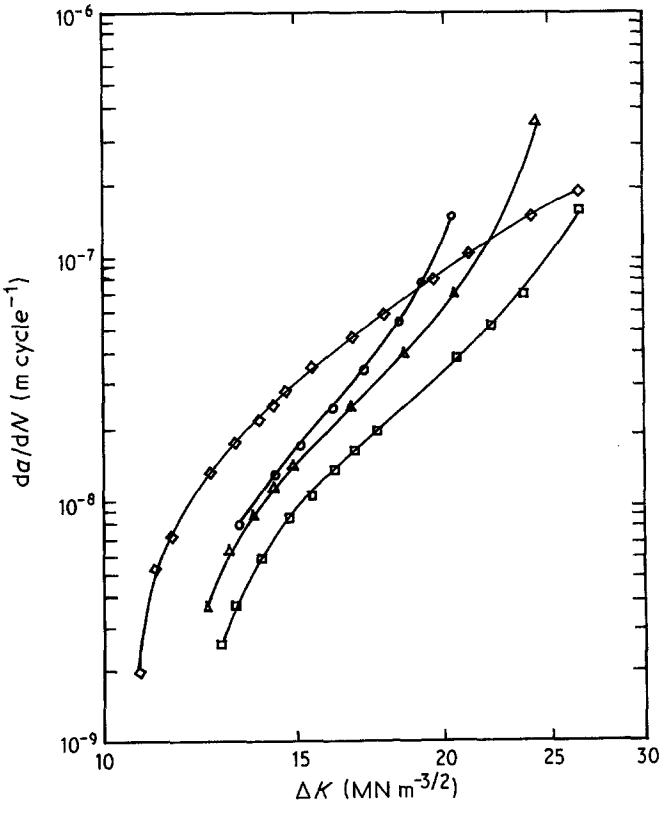

Figure 11 Plots of fatigue crack growth rate against stress intensity factor range.

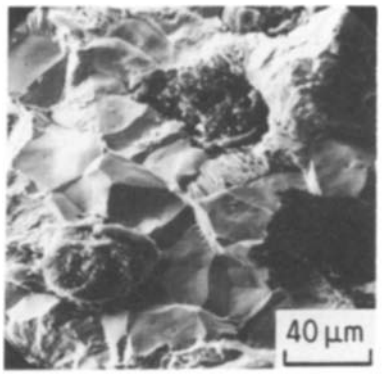

Figure 12 Intergranular cleavage of iron A at $\Delta K = 12.7\,\mathrm{MN\,m^{-3/2}}$.

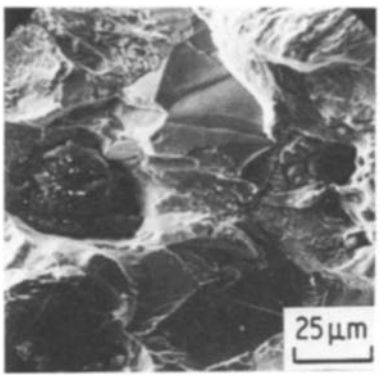

Figure 13 Mixed mode of intergranular and transgranular fracture of iron A at $\Delta K = 17.0\,\mathrm{MN\,m^{-3/2}}$.

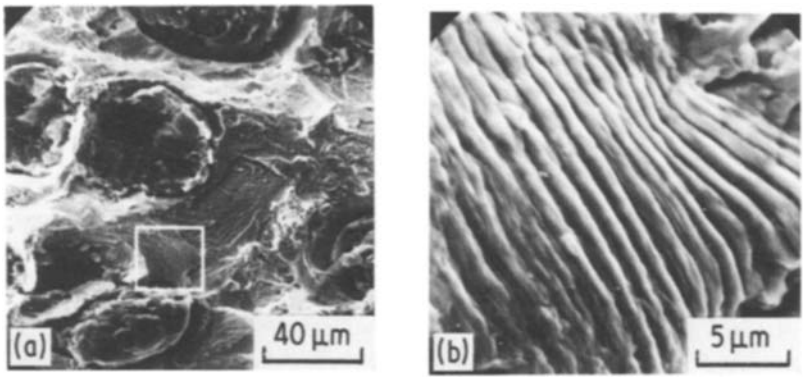

Figure 14 Fatigue striations of iron B at $\Delta K = 21.7\,\mathrm{MN\,m^{-3/2}}$. (a) Low magnification and (b) high magnification.

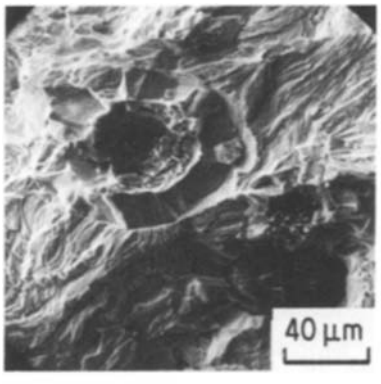

Figure 15 Fractograph of iron C at $\Delta K = 16.1\,\mathrm{MN\,m^{-3/2}}$.

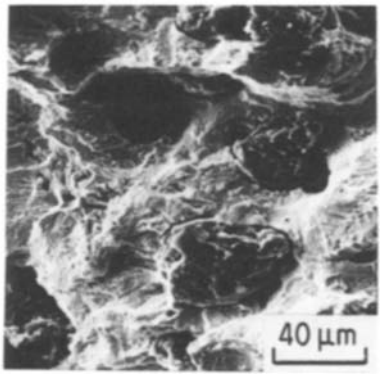

Figure 16 Fractograph of iron C at $\Delta K = 24.8\,\mathrm{MN\,m^{-3/2}}$.

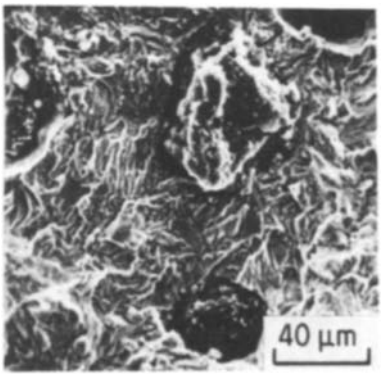

Figure 17 Fractograph of iron D at $\Delta K = 11.3\,\mathrm{MN\,m^{-3/2}}$.

4. Conclusions

1. The upper limit of the transition temperature in K_c value and the upper shelf fracture toughness increase with pearlite fraction.

2. The existence of nodular void region on fracture surfaces has an important effect on fracture toughness.

3. The exponent constant in the Paris equation decreases when the pearlite fraction increases, i.e. the fatigue crack growth rate is less sensitive to the stress intensity factor range when pearlite fraction increases.

4. For ferritic nodular cast iron, intergranular fracture occurs at low ΔK, and transgranular cleavage

fraction increases with ΔK. Striations are observed especially at higher ΔK, and the directions of striations are irregular.

5. For pearlitic nodular cast iron, the interface of the ferrite ring and pearlite colonies can be seen clearly on the fracture surface at lower ΔK, and become less distinct when ΔK increases.

Acknowledgments

The authors would like to thank the Tjing-Ling Manufacture Technique Research and Development Centre for the provision of laboratory facilities.

References

1. C. XU and R. Z. YU, *AFS Int. Cast Met. J.* **4** (1979) 21.
2. S. R. HOLDSWORTH and G. JOLLEY, *Brit. Foundryman* **68** (1975) 169.
3. W. L. BRADLEY and H. E. MEAD, "Mechanical Behaviour of Materials", Proceedings of the 3rd International Conference on Mechanical Behaviour of Materials, Cambridge, August 1979, Vol. 3 (Pergamon Press, Oxford, 1980) p. 19.
4. H. E. MEAD and W. L. BRADLEY, *AFS Trans.* **88** (1980) 265.
5. S. R. HOLDSWORTH and G. JOLLEY, *Brit. Foundryman* **67** (1974) 77.
6. R. K. NANSTAD and F. J. WORZALA, *AFS Trans.* **83** (1975) 245.
7. R. K. NANSTAD, F. J. WORZALA and C. R. LOPER, *ibid.* **82** (1974) 473.
8. J. NISKANEN, *AFS Int. Cast Met. J.* **2** (1977) 20.
9. C. W. TEN HAGEN and J. T. BERRY, *AFS Trans.* **84** (1976) 535.
10. F. J. WORZALA, R. W. HEINE and Y. W. CHENG, *ibid.* **84** (1976) 675.
11. A. LAZARIDIS, F. J. WORZALA, C. R. LOPER and R. W. HEINE, *ibid.* **79** (1971) 351.
12. B. ÖSTENSSON, *Scand. J. Metall.* **2** (1973) 194.
13. J. O. T. ADEWARA and C. R. LOPER, *AFS Cast Met. Res. J.* **11** (1975) 104.
14. *Idem, AFS Trans.* **84** (1976) 507.
15. *Idem, ibid.* **84** (1976) 513.
16. *Idem, ibid.* **84** (1976) 527.
17. P. J. RICKARDS, *J. Iron Steel Inst.* **209** (1971) 190.
18. K. V. PRABHAKAR and H. L. EWALDS, *AFS Int. Cast Met. J.* **5** (1980) 47.
19. I. S. GUZ', V. M. MATSEVITYI, S. L. MOLODTSOV and V. I. GAZOV, *Met. Sci. Heat Treatment* **21** (1979) 599.
20. J. PIRS and A. H. SHABAIK, *Fracture* **3** (1977) 819.
21. I. L. MOGFORD, I. L. BROWN and D. HULL, *J. Iron Steel Inst.* **205** (1967) 729.
22. A. G. GLOVER and G. POLLARD, *ibid.* **209** (1971) 138.
23. Y. A. SMOLYANITSKII and E. K. SAZONOV, *Met. Sci. Heat Treatment* **15** (1973) 962.
24. Y. KURODA and H. TAKADA, *AFS Cast Met. Res. J.* **6** (1970) 63.
25. T. LUYENDIJK and H. NIESWAAG, *AFS Int. Cast Met. J.* **6** (1981) 18.
26. E. S. JOHN and F. B. WILLIAM, *ASTM STP* **381** (1965) 133.
27. F. B. WILLIAM and E. S. JOHN, *ibid.* **410** (1966) 1.
28. J. R. HWANG, J. L. DOONG and H. S. CHEN, *J. Mater. Sci. Lett.* **2** (1983) 737.
29. E. HORNBOGEN and J. M. MOTZ, *AFS Int. Cast Met. J.* **2** (1977) 31.
30. L. GRÜTER, *Mater. Sci. Eng.* **35** (1978) 157.

Received 13 April
and accepted 13 May 1985